

Using the Tsallis distribution for hadron spectra in pp collisions: Pions and quarkonia at $\sqrt{s} = 5\text{--}13000$ GeV

Smbat Grigoryan*

*Joint Institute for Nuclear Research, 141980 Dubna, Russia and
A.I.Alikhanyan National Science Laboratory (YerPhI), 0036 Yerevan, Armenia*

(Dated: April 10, 2017)

A thermal model, based on the Tsallis distribution and blast-wave model, is proposed to compute hadron double-differential spectra $d^2N/dp_T dy$ in pp (also high-energy $p\bar{p}$) collisions. It successfully describes the available experimental data on pion and quarkonia (ϕ , J/ψ , $\psi(2S)$, Υ family) production at energies from $\sqrt{s} = 5$ GeV to the LHC ones. Simple parametrizations for the \sqrt{s} dependence of the model parameters are provided allowing predictions for the yields of these particles at new collision energies. The model can be used also for the pion Bose-Einstein correlation studies.

PACS numbers: 24.10.Pa, 13.85.Ni, 25.75.-q

I. INTRODUCTION

Theoretical description of the hadron transverse momentum (p_T) and rapidity (y) spectra produced in proton-proton (pp), proton-nucleus (pA) and nucleus-nucleus (AA) collisions is one of the important tasks of high-energy physics. Since its realization in the QCD is still not fully satisfactory (e.g., due to the parton hadronization complicated processes, especially at low p_T), alternative phenomenological methods are also in use. For instance, the thermal models of the stationary fireball (hadronic gas) with conventional Boltzmann-Gibbs distribution (BGD) are widely used to explain the hadronic abundances and p_T -spectra at low p_T (see, e.g., [1–4]). At high p_T the exponential BGD is not adequate since the spectra have a power-law form. The thermal models with expanding (also called flowing) fireball, like the blast-wave model (BWM) [5, 6], are included in hadron generators [7–9]. They assume the physics scenario that the initial collision creates a thermalized quark-gluon fireball, which expands, cools, hadronizes and goes through the chemical freeze-out and finally the kinetic freeze-out, when it decays into the free-streaming hadrons. Hadron spectra are computed usually by the Cooper-Frye formula [10] and flow-boosted BGD. The longitudinal flow helps us to explain the y -spectra (see, e.g., [5, 6, 11]), while the radial (or transverse) flow flattens the p_T -spectra and improves the data description up to p_T values of several GeV/ c (see, e.g., [5, 6, 12–16]).

Recent years the thermal models employing the Tsallis distribution (TD) [17] have become very popular, especially after the LHC operation [18–48]¹. Its ability to describe the charged hadron p_T -spectra in a large p_T range 0–200 GeV/ c [29–31] is very impressive. TD is a generalization of the BGD. Besides the temperature T and chemical potential μ it has an additional parameter

q and reduces to BGD in the limit $q \rightarrow 1$. TD can be considered as a result of averaging of the temperature fluctuations in the BGD, where $q - 1$ characterizes the strength of these fluctuations [20] (for other interpretations, see [34, 35]). The relation of TD with the QCD hard-scattering formulas is discussed in [30, 31]. Thanks to parameter q , TD provides a smooth transformation of the p_T -spectrum shape from the nearly exponential form at low p_T , similar to BGD, to the power-law form at high p_T , which is the usual domain of the perturbative QCD. Most of the TD-based models consider a stationary fireball and are devoted to the fits of hadron p_T -spectra in different collisions. Papers [23, 41] use a flowing fireball of the BWM and study the radial flow effect on the p_T -spectra. In [36, 39], the y -spectra of charged particles are also considered in the two-fireball models with a longitudinal flow. All these studies give different values for T and q . Parameter q increases slowly with the collision energy \sqrt{s} and varies in the range 1–1.2, depending on the hadron and collision types. Some theoretical arguments give the upper limit $q = 11/9$ [19].

In the present paper we propose a new thermal model based on the TD and BWM with a flowing fireball. It utilizes thermodynamically consistent version of the TD [24, 25] and differs from similar models by a suitable choice of the BWM ingredients (see Sec. II), allowing us to describe the shape and normalization of the hadronic p_T and y spectra, measured in pp collisions at energies from $\sqrt{s} = 5$ GeV to the highest LHC one of 13 TeV and in $p\bar{p}$ collisions at $\sqrt{s} > 500$ GeV. In our model, unlike others which also use TD, the kinetic freeze-out temperature is the same for all hadron species. Here we consider only pions and quarkonia since the pion data are the most abundant (in terms of statistics and \sqrt{s} values) and the quarkonia (J/ψ , $\Upsilon(1S)$, ...) data cover large intervals of p_T and y , which are important for our fits to better fix the model parameters. We provide simple parametrizations for the \sqrt{s} -dependence of the model parameters allowing us to predict the pion and quarkonia yields $d^2N/dp_T dy$ in pp collisions at new energies. Other particles as well as pA and AA collisions will be considered elsewhere.

The paper is organized as follows: Sec. II gives details

* Smbat.Grigoryan@cern.ch

¹ There are hundreds of papers that develop and/or use such models. We cite only some of them which include further references.

of the model. In Sec. III, we discuss the model parameters and fit procedure. Sections IV and V are devoted to the description of pion and quarkonia data, respectively. In the last section, our concluding remarks are given.

II. MODEL DESCRIPTION

In thermal models the single-particle invariant yield is usually defined by the Cooper-Frye integral over the kinetic freeze-out space-time hypersurface Σ_f [10]

$$E \frac{d^3 N}{d^3 p} = \frac{g}{(2\pi)^3} p_\nu \int_{\Sigma_f} d^3 \Sigma^\nu f(X), \quad (1)$$

where $X = (p_\nu u^\nu - \mu)/T$. Here the integrand f is the freeze-out distribution of particle four-momentum $p = (E, \vec{p})$ and four-coordinate $x = (t, \vec{x})$ with temperature T and x -dependent collective flow four-velocity u , $u_\nu u^\nu = 1$, μ is the particle chemical potential and $g = 2J + 1$ is its spin degeneracy factor. Generally, T and μ may also depend on x , but in order to keep our model as simple as possible, we assume that they are constant on the Σ_f . Then, the invariant volume V_f , which is called the fireball effective volume of particle production and includes the flow effects, could be factored out due to the Lorentz invariance in the expression for the particle total integrated yield [49–54]

$$N = \frac{g}{(2\pi)^3} V_f \int d^3 p f\left(\frac{E - \mu}{T}\right), \quad (2)$$

$$V_f = \int_{\Sigma_f} d^3 \Sigma^\nu u_\nu(x).$$

We further assume, according to the BWM [5, 6], that the fireball flow and geometry are azimuthally symmetric and boost invariant along the longitudinal (z) direction, as expected at high-energy pp (also $p\bar{p}$ and central AA) collisions. Now, instead of the Cartesian coordinates, it is convenient to introduce the radial vector $\vec{r} = (r \cos \phi, r \sin \phi)$ and the Bjorken longitudinal proper time $\tau = \sqrt{t^2 - z^2}$ and space-time rapidity $\eta = \frac{1}{2} \ln \frac{t+z}{t-z}$. Then, the flow four-velocity could be written as [5]

$$u^\nu = \gamma_r (\cosh \eta, v_r \cos \phi, v_r \sin \phi, \sinh \eta), \quad (3)$$

where $\gamma_r = 1/\sqrt{1 - v_r^2}$ and v_r is the radial flow velocity. Expressing the particle four-momentum via the y and p_T ($m_T = \sqrt{m^2 + p_T^2}$ is transverse mass), $p^\nu = (m_T \cosh y, p_T \cos \phi_p, p_T \sin \phi_p, m_T \sinh y)$, we get

$$p_\nu u^\nu = \gamma_r [m_T \cosh(y - \eta) - v_r p_T \cos(\phi_p - \phi)]. \quad (4)$$

The hypersurface Σ_f in the BWM is defined by the condition that the freeze-out happens at a constant value of the proper time: $\tau = \tau_f = \text{const.}$ In this case the hypersurface element four-vector has a simple form [6, 8]

$$d^3 \Sigma^\nu = \tau_f (\cosh \eta, 0, 0, \sinh \eta) d\eta d^2 r. \quad (5)$$

We fix the Σ_f geometry as follows: in the longitudinal direction, it is limited in the interval $-\eta_{max} < \eta < \eta_{max}$, where a maximum longitudinal flow rapidity η_{max} is required by the finite total energy (this breaks the exact longitudinal boost invariance). In the radial direction the upper boundary of r is given by radius $R(\eta)$ that depends on η . This dependency plays a major role in our model for the proper description of the hadron rapidity spectra. We have tried different forms for it and found that the following simple one (see, e.g., [6])

$$R(\eta) = R_0 \sqrt{1 - \eta^2 / \eta_{max}^2} \quad (6)$$

is very successful. Since R_0 is the radius at $\eta = 0$, the fireball gets thinner with increase of $|\eta|$.

Now, we need to define the radial flow velocity v_r . Usually one assumes that it equals zero at $r = 0$ and grows with r according to a power-law dependence [5]. We have found that the simple quadratic dependency

$$v_r(r) = v_s \cdot (r/R_0)^2 \quad (7)$$

allows us to correctly describe the hadron p_T spectra. Here $v_s = v_r(R_0)$ is the surface velocity. A useful quantity is the mean value of $v_r(r)$, which can be defined as

$$\langle v_r \rangle = \frac{1}{V_f} \int_{\Sigma_f} d^3 \Sigma^\nu u_\nu(x) v_r(r). \quad (8)$$

According to the Eqs. (2)–(7) one has

$$V_f = \tau_f \int_{-\eta_{max}}^{\eta_{max}} d\eta \int_0^{R(\eta)} \gamma_r r dr \int_0^{2\pi} d\phi$$

$$= \frac{3}{2} \frac{V_0}{v_s} \int_0^1 dx \arcsin[v_s(1 - x^2)], \quad (9)$$

where $V_0 = 4/3 \pi R_0^2 \tau_f \eta_{max}$. Performing similar calculations with Eq. (8) we obtain

$$\langle v_r \rangle = \frac{3}{2} \frac{V_0}{V_f} \int_0^1 dx (1 - 3x^2) \arcsin[v_s(1 - x^2)]. \quad (10)$$

Fig. 1 shows that the ratios V_f/V_0 and $\langle v_r \rangle / (0.4 v_s)$ are equal unity at $v_s = 0$ and grow with the v_s .

Thus, we defined the BWM ingredients of our model. Now we specify the function f in Eq. (1) by choosing the thermodynamically consistent TD [24, 25] (in contrast to the TD version, defined by Eq. (11) with the external power index -1 instead of $-q$)

$$f(X) = \left[[1 + (q - 1)X]^{\frac{1}{q-1}} - \xi \right]^{-q}, \quad (11)$$

where ξ equals 1 or -1 to account for the quantum statistics of bosons or fermions, respectively. This quantum correction matters only for pions due to their small mass. Expanding the right-hand side of Eq. (11) into the binomial series and substituting it in Eq. (1), one gets

$$E \frac{d^3 N}{d^3 p} = \frac{d^3 N}{d^2 p_T dy} = \frac{g \tau_f}{(2\pi)^3} \sum_{k=0}^{\infty} \xi^k \binom{q-1+k}{k} \times$$

$$\int_{-\eta_{max}}^{\eta_{max}} d\eta \int_0^{R(\eta)} r dr \int_0^{2\pi} d\phi \frac{m_T \cosh(y - \eta)}{[1 + (q - 1)X]^{\frac{q+k}{q-1}}}. \quad (12)$$

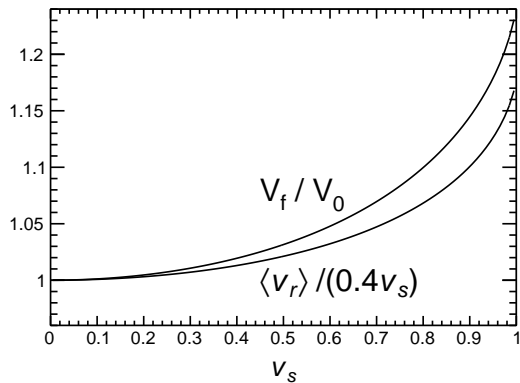


FIG. 1. Ratios V_f/V_0 and $\langle v_r \rangle/(0.4v_s)$ depending on v_s .

Using Eq. (4) and performing integrations over ϕ and ϕ_p (second integration gives 2π), we obtain

$$\frac{d^2N}{p_T dp_T dy} = g \frac{3V_0}{8\pi^2} \sum_{k=0}^{\infty} \xi^k \binom{q-1+k}{k} \int_{-\eta_{max}}^{\eta_{max}} \frac{d\eta}{\eta_{max}} \times \int_0^{R(\eta)} \frac{r dr}{R_0^2} \frac{m_T \cosh(y-\eta) a^{\frac{q+k}{q-1}}}{[1 + \frac{\gamma_r m_T \cosh(y-\eta) - \mu}{T/(q-1)}]^{\frac{q+k}{q-1}}} P_{\frac{k+1}{q-1}}(a), \quad (13)$$

where $a = 1/\sqrt{1-b^2}$,

$$b = \frac{\gamma_r v_r p_T}{T/(q-1) + \gamma_r m_T \cosh(y-\eta) - \mu}$$

and $P_\nu(a)$ is the Legendre function of the first kind [55]. Taking into account the relation ($I_0(x)$ is the modified Bessel function)

$$\lim_{q \rightarrow 1} a^{\frac{k+1}{q-1}} P_{\frac{k+1}{q-1}}(a) = I_0\left(\frac{k+1}{T} \gamma_r v_r p_T\right)$$

one can easily verify that in the limit $q \rightarrow 1$ Eq. (13) reproduces usual BWM formulas [6] based on the BGD. Eq. (13) (with Eqs. (6) and (7)) is the main formula of our model. We have checked that the series in this formula is convergent if $\mu < m$ (like for similar series in the thermal models with BGD [4]). This condition is fulfilled according to Eqs. (21) and (22). Higher terms of the series are important only for pions (mostly for π^+ which has larger μ) at low values of \sqrt{s} , $|y|$ and p_T . For example, for the case of $\sqrt{s} = 30.6$ GeV, $y = 0$ and $p_T \sim 0$, considered in Sec. IV, first three terms of the series give together about 97% of the π^+ yield. At lower energies, more terms of the series should be used for the accurate computation of pion yields. For heavier hadrons, one can safely use $\xi = 0$.

III. PARAMETERS AND FIT PROCEDURE

Here, we utilize Eq. (13) for fitting the hadron spectra in pp and $p\bar{p}$ collisions. We follow two aims. First is to

show that our model with a possibly minimum number of parameters is able to describe well the available data on p_T and y spectra for different particles and energies \sqrt{s} . The second aim is to systematize the fit results for different \sqrt{s} and provide simple parametrizations for the \sqrt{s} -dependence of model parameters, permitting predictions for the future experiments.

To fit the data given in terms of the cross section σ , we convert it to the invariant yield N via the relation $\sigma = N\sigma_{in}$, where σ_{in} is the pp or $p\bar{p}$ inelastic cross section at the energy \sqrt{s} /GeV (λ equals 1 or -1 , respectively, see the L2 model of Table B1 in [56])

$$\sigma_{in} = (26.2 + 0.1717 \ln^2 \frac{s}{3.521} + \frac{53.2}{s^{0.40}} - \frac{27.0}{s^{0.48}} - \lambda \frac{33.8}{s^{0.545}}) \text{mb}. \quad (14)$$

As in other applications of TD for inclusive pions, we do not calculate explicitly the feed-down contribution from the resonance decays, assuming that directly produced pions and secondary ones have the same spectral shapes. Secondary pions are expected to dominate at low p_T (see, e.g., [12]).

Eq. (13) has six independent parameters: T , q , μ , V_0 , η_{max} and v_s . Generally, they can depend on the \sqrt{s} and hadron type. We assume that the kinetic freeze-out temperature T is the same for all hadron species (the chemical freeze-out temperature may rise with the hadron mass). Since the neutral pions and quarkonia (ϕ , J/ψ , $\psi(2S)$, Υ family) do not have conserved quantum numbers, their chemical potential μ must equal zero in the chemical equilibrium [1]. We have verified that at $\sqrt{s} > 50$ GeV the neutral and charged pion data can be successfully fitted with $\mu = 0$, while this is not true for heavier hadrons. The nonzero μ can be interpreted as a measure of the non-equilibrium for the given particle. A similar fact is well known in the non-equilibrium thermal models based on BGD, where one introduces so-called phase-space occupancy γ , related to the chemical potential as $\mu = T \ln \gamma$ [4]. To ensure the same yield for the pion three charge states at high energies, as follows from the data, we assume that all the model parameters, except μ , are the same for these states. Moreover, we will use for them a common averaged mass $m_\pi = (2m_{\pi^\pm} + m_{\pi^0})/3$.

Using the above-mentioned assumptions, we have done χ^2 fits (in the ROOT framework [57]) of the existing data on pion and quarkonia p_T spectra for different values of y and \sqrt{s} . We started with the pion fits and have observed that parameter T increases with energy at low energies up to about $\sqrt{s} = 10$ GeV. Then, it decreases and becomes practically constant at $\sqrt{s} > 500$ GeV. This behavior can be parametrized as (see Fig. 2)

$$T = T_\infty \left(1 + \frac{1.33\sqrt{x} - 0.21}{1 + x^2}\right), \quad (15)$$

where $x = \sqrt{s}/(16 \text{ GeV})$ and $T_\infty = 78 \text{ MeV}$ is the temperature at $\sqrt{s} \rightarrow \infty$. Similar energy dependence was observed for the kinetic freeze-out temperature in AA

collisions using thermal models with the BGD (see, e.g., Fig. 11a in [15]).

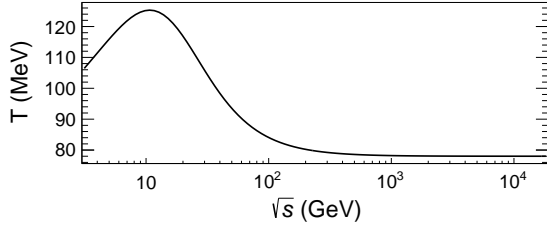


FIG. 2. Kinetic freeze-out temperature T depending on \sqrt{s} .

We then utilized Eq. (15) in the fits of all hadrons. The fit results for η_{max} and v_s are parametrized as

$$\eta_{max} = 0.89y_m - 0.32 - 1.18 \frac{y_m}{y_b} + \frac{1.86}{y_b} - \frac{0.17}{y_m} - 0.025 \frac{m_p}{m} e^{-\sqrt{s}/e_0}, \quad (16)$$

$$v_s = 0.78(1 - \frac{1.31}{y_m} - \frac{0.09}{y_m} \frac{m}{m_p} - \frac{0.023}{y_b} \frac{m_p}{m}), \quad (17)$$

where $e_0 = 45$ GeV, m is the mass of given hadron, $y_m = \ln(\sqrt{s}/m)$ its maximum rapidity, m_p the proton mass and $y_b = \ln(\sqrt{s}/m_p)$ the beam rapidity in high energy pp or $p\bar{p}$ collisions. In our model, the y -spectrum width is proportional to η_{max} and grows logarithmically with \sqrt{s} . Besides, the larger m is, the smaller η_{max} is and hence the narrower the y -spectrum is. Parameter v_s changes in the range 0–0.78, increases with \sqrt{s} and decreases with increasing m . Eqs. (10) and (17) show that radial flow velocity for pions is significant even at $\sqrt{s} \sim 5$ GeV (while it vanishes at $\sqrt{s} \leq 540$ GeV in [23]). Note that the last terms in Eqs. (16) and (17) are important only for pions at low energies.

The remaining fit parameters also demonstrate properties common for different hadrons. The volume parameter can be expressed as

$$V_0 = \tilde{V} \eta_{max} y_b (T_\infty/T)^{2.06}, \quad (18)$$

where \tilde{V} is \sqrt{s} -independent but strongly decreases with increase of the hadron mass (see Table I)². Note that

² In principle, it is possible to redefine the Eq. (13) parameters and obtain for heavier hadrons the same \tilde{V} as for pions using the following identity transformation of the TD (see also [26]):

$$\tilde{V} [1 + \frac{E - \mu}{T/(q-1)}]^{1-\frac{q}{q-1}} = \tilde{V}_\pi [1 + \frac{E - \mu'}{(T - T\delta)/(q-1)}]^{1-\frac{q}{q-1}},$$

where $\mu' = \mu - T\delta/(q-1)$ and parameter $\delta = 1 - (\tilde{V}/\tilde{V}_\pi)^{1-1/q}$ grows with \tilde{V}_π/\tilde{V} . As mentioned in Sec. I, the $q-1$ characterizes the temperature fluctuations around the mean value T . According to [21], the quantity $T\delta$ can be interpreted as a measure of the energy transfer, caused by these fluctuations, from the fireball region where the particle is produced to the surrounding regions. Note that $\delta \sim (q-1)$ at $q \rightarrow 1$, as expected in [21].

TABLE I. Parameters of Eqs. (18)–(21) for $\pi^{\pm,0}$, ϕ , J/ψ , $\psi(2S)$ and $\Upsilon(1S)$, obtained from the combined fits of data measured at different energies. The χ^2 and NDF correspond to the fits when all the parameters, except \tilde{V} , are fixed to their central values. Additional parameters for higher Υ states and non-prompt J/ψ and $\psi(2S)$ production are given in Sec. V.

	π	ϕ	J/ψ	$\psi(2S)$	$\Upsilon(1S)$
\tilde{V} (GeV ⁻³)	5030.9	561.2	107.4	19.2	0.241
e_1 (GeV)	± 7.2	± 5.2	± 0.4	± 0.1	± 0.001
p_1	12.5	12.5	7.8	7.8	30.0
p_2	3.5	3.5	76.1	128.1	0
p_3	2.3	3.1	0	0	0
p_4	135.6	166.3	56.3	56.3	3.0
p_5	0	0	29.2	29.2	8.6
p_6	46.7	46.7	87.9	94.0	-4.3
e_2 (GeV)	-	8786	13900	35500	$1 \cdot 10^9$
e_3 (GeV)	-	225	63.1	63.1	16000
p_7	-	0.047	0.072	0.060	0.058
χ^2	-	2.30	2.01	0.50	3.50
NDF	8716	235	5985	1567	5773
	2293	223	1707	974	622

$V_0 \sim \ln^2 s$ at high \sqrt{s} . The normalization constant \tilde{V} for inclusive pions, given in Table I, includes the contribution of the resonance decays and hence is expected to be larger than the one for the directly produced pions.

The fitted values of q grow with \sqrt{s} and are different for different hadron species. However they vary in the very small interval 1–11/9, as noted in Sec. I. Therefore, it is more convenient to use the parameter n instead

$$n = q/(q-1), \quad (19)$$

which controls the large- p_T behavior of Eq. (13). Then, $n > n_\infty = 11/2$ [19] and $n \rightarrow \infty$ at $q \rightarrow 1$. The resulting fitted values of n can be parametrized for different hadron species by the formula, valid at $x = e_1/\sqrt{s} < 1$,

$$n = \frac{n_\infty}{1 + p_1 x} + \frac{p_3/\ln x}{\ln x - p_2} + p_4 x^{0.37} - p_5 x, \quad (20)$$

where parameters e_1 and p_1 – p_5 are listed in Table I and e_1

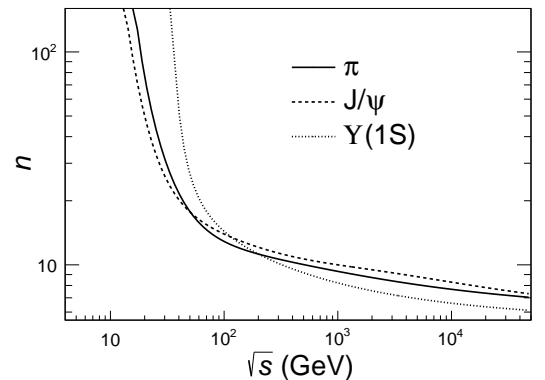


FIG. 3. Parameter n for π , J/ψ and $\Upsilon(1S)$ depending on \sqrt{s} .

is the energy when n becomes infinity. So, at $\sqrt{s} \leq e_1$, the TD reduces to BGD. The limiting value n_∞ provides that Eq. (13) at $\sqrt{s} \rightarrow \infty$ has the same large- p_T behavior as the jet production in the lowest-order perturbative QCD [31]. Fig. 3 shows the energy dependence of n for π , J/ψ and $\Upsilon(1S)$. The corresponding curves for ϕ , $\psi(2S)$ and higher Υ states are similar to the ones for π , J/ψ and $\Upsilon(1S)$, respectively.

The obtained values of μ are always smaller m . They are proportional to m and vanish with increasing \sqrt{s} . We parametrize μ for different quarkonium species by the formula, valid at $\sqrt{s} \leq e_2$,

$$\mu = p_6 \left(\ln \frac{e_2}{\sqrt{s}} - p_7 \frac{1 - \sqrt{s}/e_2}{1 + \sqrt{s}/e_3} \right) m, \quad (21)$$

where parameters e_2 , e_3 , p_6 and p_7 are given in Table I and $\mu = 0$ at $\sqrt{s} > e_2$ (e_2 is larger for heavier particles). For pions we use

$$\mu_\pi = \frac{2 \text{ GeV}}{\sqrt{s}} (1 + 0.6 Q_\pi) e^{-\sqrt{s}/e_0} m_\pi, \quad (22)$$

where $Q_\pi = 0$ for $p\bar{p}$ collisions while for pp collisions Q_π

equals the pion charge, to account for the difference of π^+ , π^0 and π^- yields in low energy pp collisions, related to the charge-conservation effects. μ_π vanishes with increasing energy, in agreement with the fact that these yields almost coincide at $\sqrt{s} \geq 62.4$ GeV [44, 45].

In Sections IV and V we will discuss in more detail the results of combined fits of pion and quarkonia data using Eqs. (13)–(22). The parameter values as well as the χ^2 and NDF of the fits for each hadron type are given in Table I. Additional parameters for J/ψ and $\psi(2S)$, produced via bottom hadron decays, and for higher Υ states will be considered in Sec. V. Note that rather large ratios χ^2/NDF are due to the large amount of data included in the fits, which use \sqrt{s} -dependent parametrizations for the model parameters. Since the quality and normalization of different measurements for given hadron do not always agree well with each other, the combined fit gives larger χ^2/NDF than the individual fits for each measurement. To get not-too-large χ^2/NDF , we have excluded some data samples from the combined fits.

IV. NEUTRAL AND CHARGED PIONS

Here, we present the results of the combined fit of

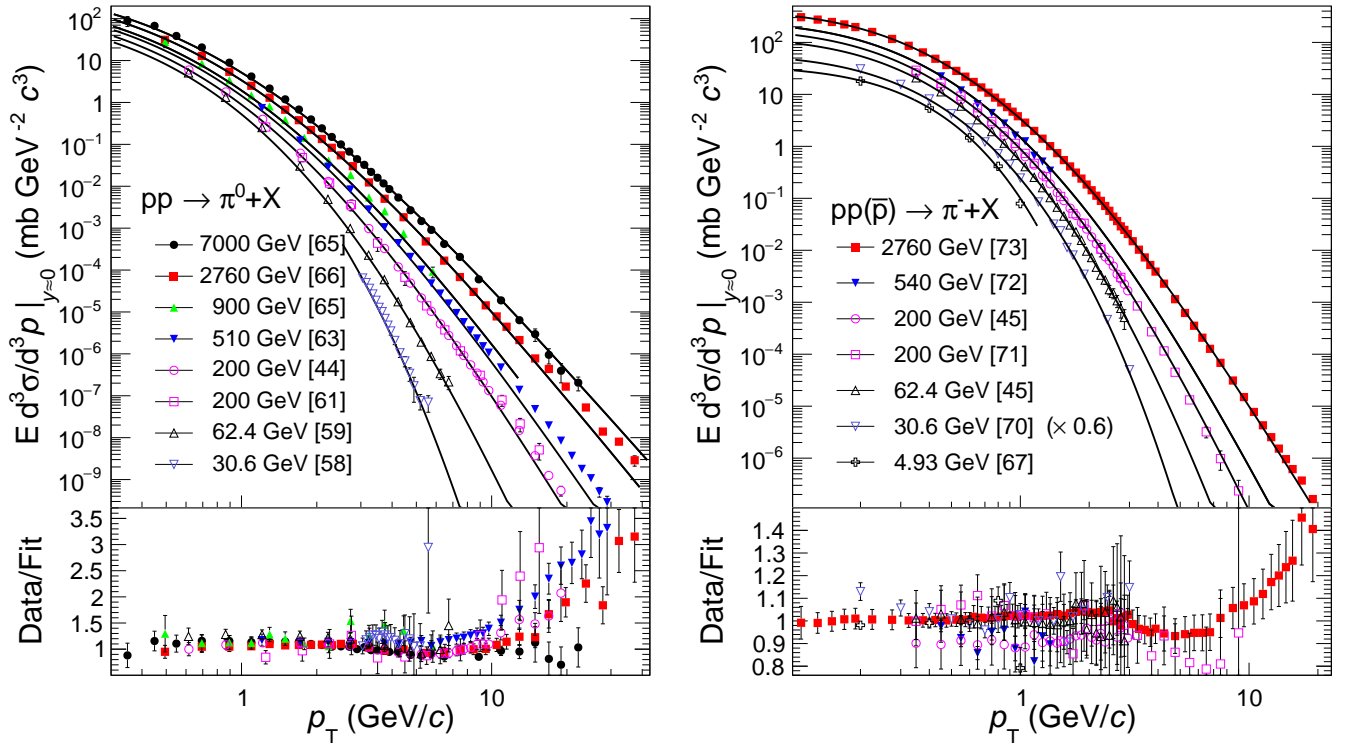


FIG. 4. (color online) Fitting of invariant cross section vs p_T at mid-rapidity and different \sqrt{s} values for π^0 (left) and π^- (right) production in pp ($p\bar{p}$ at $\sqrt{s} = 540$ GeV) collisions. Symbols represent the data points and the line is the fit function. The π^- data and line at $\sqrt{s} = 30.6$ GeV are multiplied by 0.6 for a better visibility. The ratios data/fit are shown at the bottom.

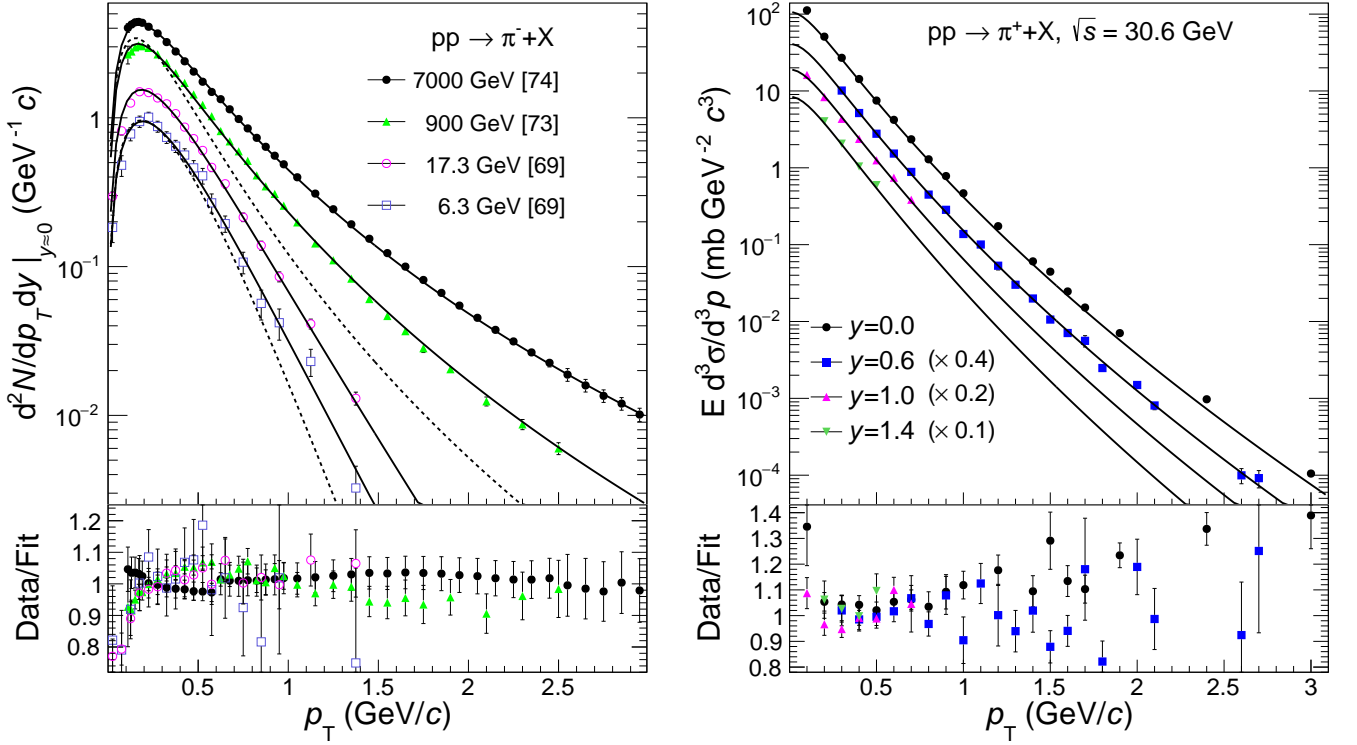


FIG. 5. (color online) Fitting of π^- invariant yield vs p_T at mid-rapidity and different \sqrt{s} values (left) and π^+ cross section vs p_T at $\sqrt{s} = 30.6$ GeV and different rapidity values [70] (right). Data and lines at $y = 0.6, 1.0, 1.4$ are multiplied by 0.4, 0.2, 0.1, respectively, for a better separation. Dashed lines show the fit functions at $\sqrt{s} = 6.3$ and 900 GeV for $v_s = 0$.

π^0 [44, 58–66] and π^\pm [45, 48, 67–74] inclusive production p_T -spectra measured for different values of y at energies \sqrt{s} from 30.6 GeV [58] to 7 TeV [66] for π^0 and from 4.93 GeV [67] to 7 TeV [48] for π^\pm . The used charged pion data are mostly for π^- . High-energy data at $\sqrt{s} = 0.54, 2.76$ and 7 TeV are for the averaged $(\pi^- + \pi^+)/2$ production. From [58], we included in the fit only the data obtained with so-called retracted geometry, and from [70], we included only the data measured at $\sqrt{s} = 30.6, 44.6$ and 52.8 GeV which cover larger intervals of p_T and y . We did not include in the fit the π^+ p_T -spectra from [67], which give too large χ^2 ; however, our model describes well the corresponding p_T -integrated data (see Fig. 6). Since the charged pion measurement at $\sqrt{s} = 200$ GeV by the STAR Collaboration [71] is for the non-single diffractive (NSD) yield, it was converted to an inclusive cross section using $\sigma_{NSD} = 30$ mb [71]. Figures 4 and 5 (left) show examples of the fits of pion p_T -spectra for mid-rapidity and different \sqrt{s} values while Fig. 5 (right) shows fits for different values of rapidity at $\sqrt{s} = 30.6$ GeV [70]. To demonstrate the quality of the fits, the data points have been divided by the corresponding values of the fit function, and the ratios are also plotted. Generally, the quality is always good. Only the π^0 data [61, 63] show a large excess at $p_T > 10$ GeV/c.

In Fig. 5 (left), the dashed lines represent the fit functions at $\sqrt{s} = 6.3$ and 900 GeV for $v_s = 0$ to illustrate the importance of the radial flow in our model.

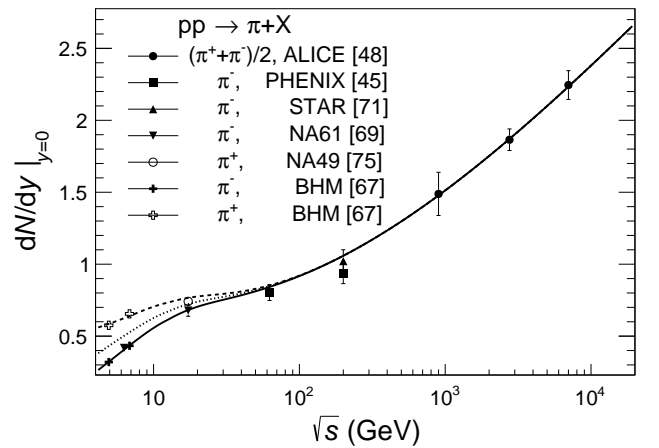


FIG. 6. Prediction for π^- (full line), π^0 (dotted line) and π^+ (dashed line) p_T -integrated invariant yields at mid-rapidity depending on \sqrt{s} and comparison with the available data.

Note that we did not include in the combined fit the π^\pm high-statistics data [75] measured in pp collisions at $\sqrt{s} = 17.3$ GeV since the published results do not quote the dominant systematic uncertainties. But we included the π^- measurement at the same energy [69], and both data sets agree well, as shown in [69]. We also did not use for the combined fit the charged pion data measured at $\sqrt{s} = 200$ GeV and high rapidities $y = 2.95$ and 3.3 [76] but have checked that our model describes them well at $p_T < 2.5$ GeV/c. At higher p_T , corresponding to pion energies larger than 25 GeV, the model overestimates the data. So, our model is not valid for such high rapidities at $\sqrt{s} = 200$ GeV, related to diffractive processes, which is generally expected for a thermal model. Note also that the π^\pm data [70] provide a large contribution into the χ^2 and NDF values shown in Table I. A combined fit without these data gives $\chi^2/NDF = 5959/1734$.

Fig. 6 presents an example of our predictions, based on Eqs. (13)–(22), for the pion p_T -integrated yields in pp collisions at mid-rapidity and varying \sqrt{s} . It shows a good agreement with the available data.

V. QUARKONIA (ϕ , J/ψ , $\psi(2S)$, $\Upsilon(1S)$ – $\Upsilon(3S)$)

A. ϕ meson

The following results are for the combined fit of ϕ meson inclusive production data measured in pp collisions at $\sqrt{s} = 17.3$ GeV [77], 200 GeV [44, 78], 900 GeV [79], 2.76 TeV [80], 7 TeV [81–83] and in $p\bar{p}$ collisions at $\sqrt{s} = 1.96$ TeV [84]. The p_T -spectrum from [85] is not included in the fit since its normalization is about six times lower the one in [84] at similar energy. It appeared that the fitted values of the ϕ meson n parameter at different \sqrt{s} are close to the pion ones. So, in the parametrization Eq. (20) for ϕ , we have fixed some of the parameter values to the ones for pion (see Table I). Examples of the p_T -spectra fits are shown in Fig. 7 for mid-rapidity and different \sqrt{s} values (left) and for different values of y at $\sqrt{s} = 7$ TeV (right). As an example of our predictions, Fig. 8 presents the ϕ meson p_T -integrated cross section in pp (also $p\bar{p}$) collisions versus \sqrt{s} at mid-rapidity and

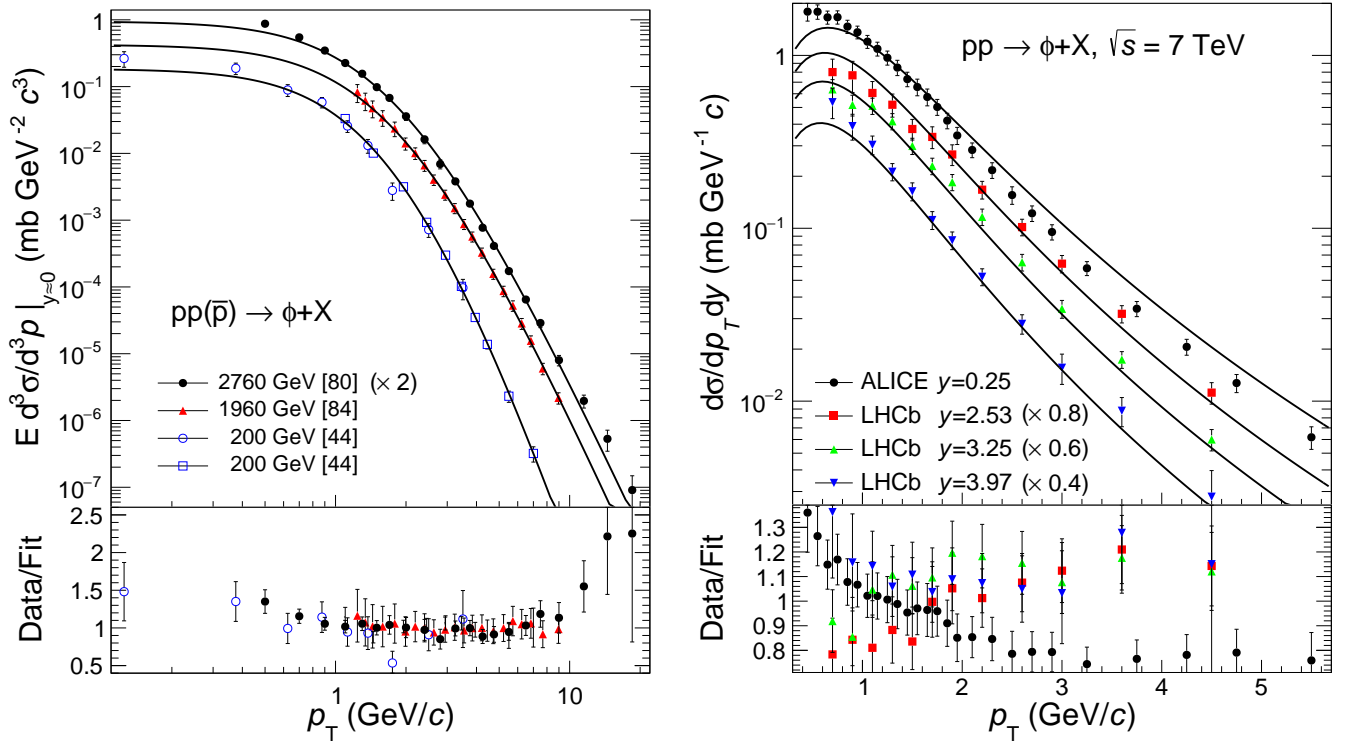


FIG. 7. (color online) Fitting of ϕ meson cross section vs p_T at mid-rapidity and different \sqrt{s} values (left) and at $\sqrt{s} = 7$ TeV and different rapidity values [81, 82] (right). The data and line for $\sqrt{s} = 2760$ GeV are multiplied by 2 and the ones for $y = 2.53, 3.25, 3.97$ are multiplied by 0.8, 0.6, 0.4, respectively, for a better separation.

at forward rapidity of $y = 3.25$ (for dimuon decay channel measurements of LHCb [81] and ALICE [80, 83]). At

$y = 3.25$ two values for the p_T -integration lower limit are considered: 0 and 1 GeV/c. Comparison of calculations

with the available data shows a reasonable agreement.

B. J/ψ meson

The inclusive J/ψ production consists of prompt component (includes direct production and feed-down from the radiative decays of higher charmonium states) and non-prompt component (includes feed-down from the weak decays of bottom hadrons). Fraction of the non-prompt component, denoted usually by f_B , is negligible at $\sqrt{s} < 100$ GeV but rises monotonically with \sqrt{s} and p_T . For LHC energies it reaches values about 0.1 at low p_T and larger values at high p_T (see Fig. 11). The kinematic distributions of prompt and direct J/ψ are similar and can be described by the same values of parameters in Eq. (13). Only the normalization constants \tilde{V} will differ. The non-prompt J/ψ has a significantly harder p_T spectrum and narrower y spectrum. Its proper description would require the use of Eq. (13) for the production of bottom mesons and baryons which have several decay channels into J/ψ . To avoid such a complex computation for a rather small fraction of data, we have chosen a simpler approach. Namely, for non-prompt J/ψ , we use Eq. (13) with the same T , n , μ and v_s parameters as for prompt J/ψ . To describe the harder p_T -spectrum of non-prompt J/ψ , we assume that the mass in m_T in the

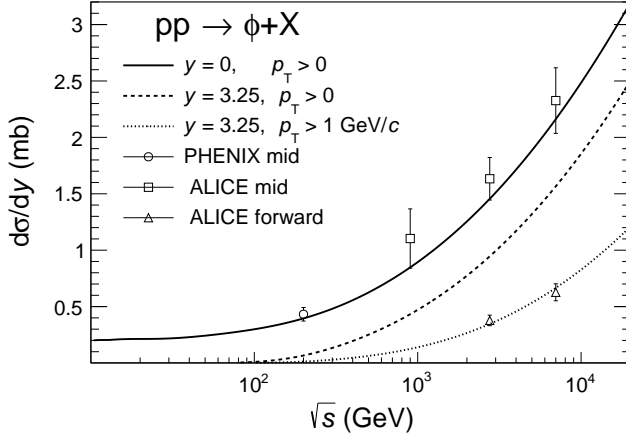


FIG. 8. ϕ meson p_T -integrated cross section at mid-rapidity (full line) and forward rapidity of $y = 3.25$ for $p_T > 0$ (dashed line) and $p_T > 1$ GeV/c (dotted line) vs \sqrt{s} . Data are from PHENIX [44], ALICE [79, 80, 82] for mid-rapidity and ALICE [80, 83] for forward rapidity at $p_T > 1$ GeV/c.

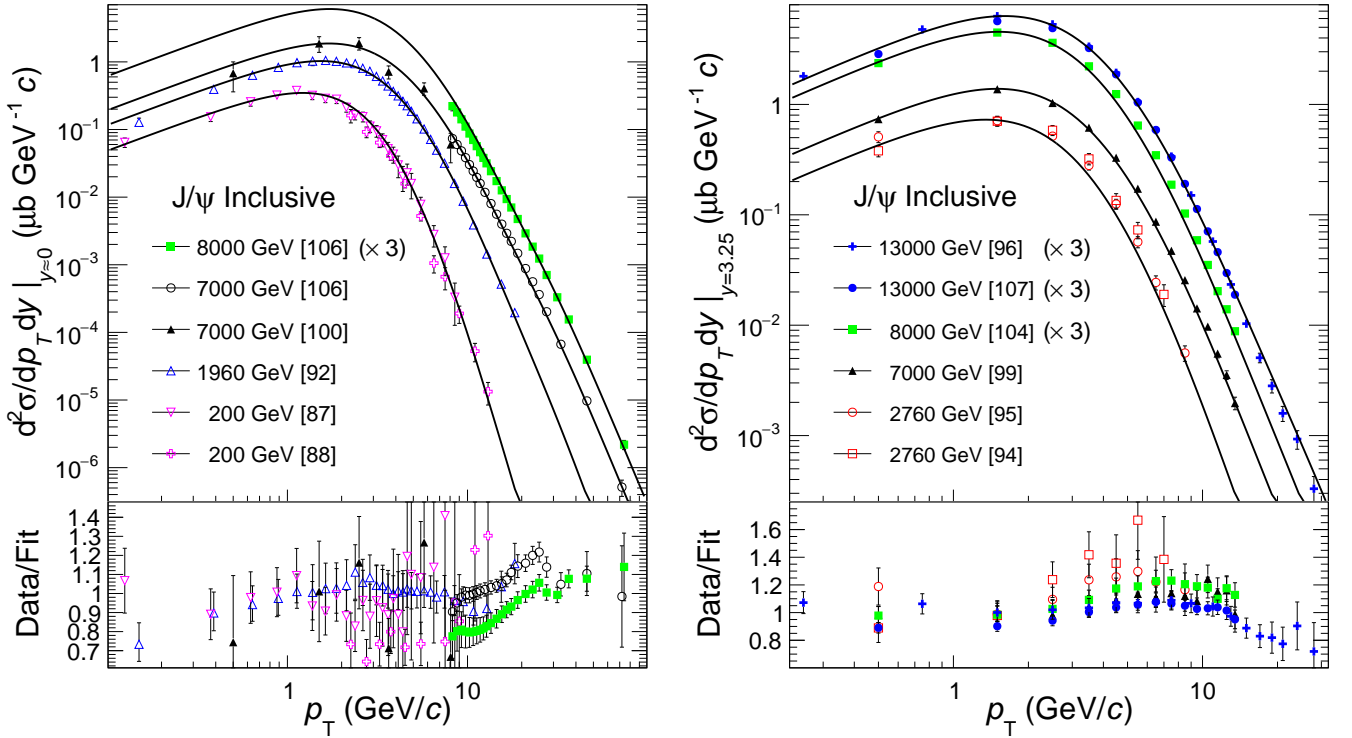


FIG. 9. (color online) Fitting of inclusive J/ψ meson cross section vs p_T at different \sqrt{s} values for mid-rapidity (left) and forward rapidity of $y = 3.25$ (right). Data and lines at $\sqrt{s} = 13, 8$ TeV are multiplied by 3 for a better visibility.

corresponding Eq. (13) is larger the J/ψ mass by some factor c_m and the normalization grows with p_T according to the parametrization

$$\tilde{V} = \tilde{V}_{NP}(1 + \frac{c_1}{1 + (c_2/p_T)^4}), \quad (23)$$

where \tilde{V}_{NP} , c_1 , c_2 and c_m are fit parameters. Also, to ensure the narrowness of the non-prompt y -spectrum, we multiply the corresponding η_{max} in Eq. (17) by another fit parameter $c_\eta < 1$. We have performed a combined fit of the available prompt and non-prompt or inclusive J/ψ production p_T -spectra [86–107] measured at energies \sqrt{s} from 19.4 GeV [86] to 13 TeV [96, 107] in pp collisions and at 1.8 TeV [89–91] and 1.96 TeV [92] in $p\bar{p}$ collisions. The p_T -spectrum from [108] is not included in the fit since its normalization is a factor of 2.5 lower than expected within our model, which however describes well the shape of this spectrum. The fit gives, in addition to the values for the model parameters, χ^2 and NDF listed in Table I, the following values for the non-prompt component parameters: $\tilde{V}_{NP} = 82.1 \pm 0.7 \text{ GeV}^{-3}$, $c_1 = 2.1$, $c_2 = 26.3 \text{ GeV}$, $c_m = 1.4$, $c_\eta = 0.82$.

We illustrate then some results of the fit. Inclusive J/ψ p_T -spectra at different \sqrt{s} values are shown in Fig. 9 for midrapidity (left) and forward rapidity of $y = 3.25$

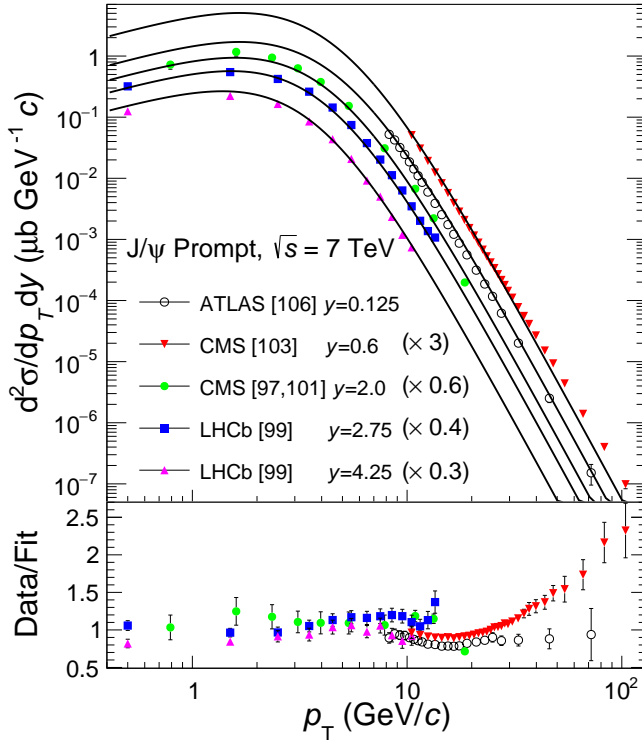


FIG. 10. (color online) Fitting of prompt J/ψ meson cross section vs p_T at $\sqrt{s} = 7 \text{ TeV}$ and different rapidity values. Data and lines at $y = 0.6, 2.0, 2.75, 4.25$ are multiplied by 3, 0.6, 0.4, 0.3, respectively, for a better separation.

(right). Data points of ATLAS [106] in Fig. 9 correspond to $0.25 < |y| < 0.5$. Figure 10 shows the prompt J/ψ p_T spectra for different rapidity values at $\sqrt{s} = 7 \text{ TeV}$. In Fig. 11, our predictions for the p_T dependence of the J/ψ non-prompt fraction at different \sqrt{s} are compared with existing published data. We demonstrate also a good agreement of our predictions with the available data on the inclusive J/ψ meson p_T -integrated cross section (for $p_T > 0$) as a function of y at three \sqrt{s} values (Fig. 12) and as a function of \sqrt{s} at mid-rapidity and forward rapidity (Fig. 13).

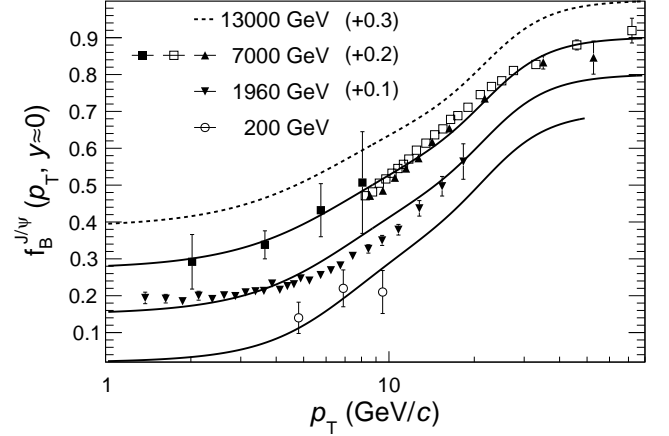


FIG. 11. Fraction of non-prompt J/ψ production versus p_T at mid-rapidity and different \sqrt{s} . Data and lines at $\sqrt{s} = 13 \text{ TeV}, 7 \text{ TeV}$ [100, 101, 106], 1.96 TeV [92], 0.2 TeV [88] are shifted up by 0.3, 0.2, 0.1, 0, respectively, for a better separation.

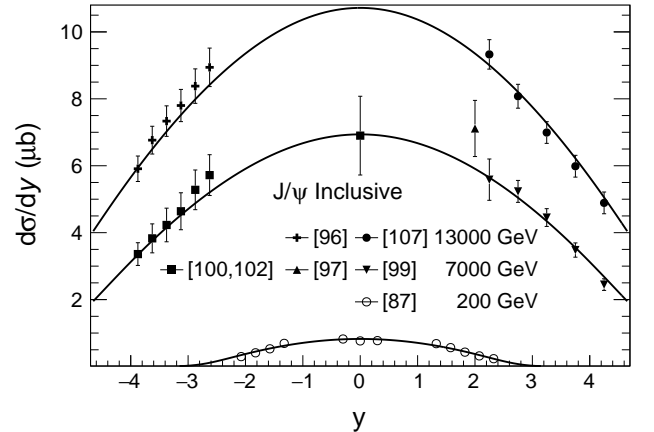


FIG. 12. Inclusive J/ψ meson p_T -integrated cross section as a function of y at different \sqrt{s} and comparison with the data.

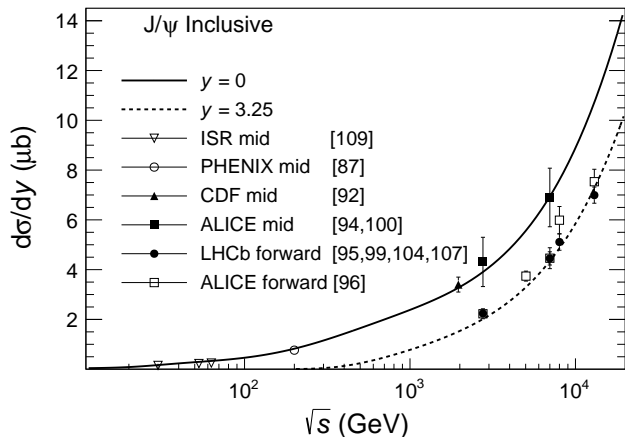
C. $\psi(2S)$ meson

FIG. 13. Inclusive J/ψ meson p_T -integrated cross section as a function of \sqrt{s} at mid-rapidity (full line) and forward rapidity of $y = 3.25$ (dashed line) and comparison with the data.

As $\psi(2S)$ is a charmonium state, similar to J/ψ , its production prompt and non-prompt components can be described similarly using Eqs. (13) and (23) (where m now is the $\psi(2S)$ mass) and parameters c_m , c_η . We have performed a combined fit of the available prompt and non-prompt or inclusive $\psi(2S)$ production data measured in pp collisions at $\sqrt{s} = 200$ GeV [87], 7–13 TeV [96, 101–103, 105, 106, 110, 111] and in $p\bar{p}$ collisions at $\sqrt{s} = 1.8$ TeV [89], 1.96 TeV [112]. The resulting fit parameter values are listed in Table I (some of them are fixed to the corresponding values of J/ψ). Additional parameters for the non-prompt $\psi(2S)$ are: $\tilde{V}_{NP} = 15.9 \pm 0.1$ GeV $^{-3}$, $c_m = 1.3$, and c_1, c_2, c_η coincide with the ones of J/ψ . Examples of the p_T -spectra fits are shown in Fig. 14 for mid-rapidity and different \sqrt{s} values (left) and for different values of y at $\sqrt{s} = 7$ TeV (right). Data points of ATLAS [106] in the left panel correspond to

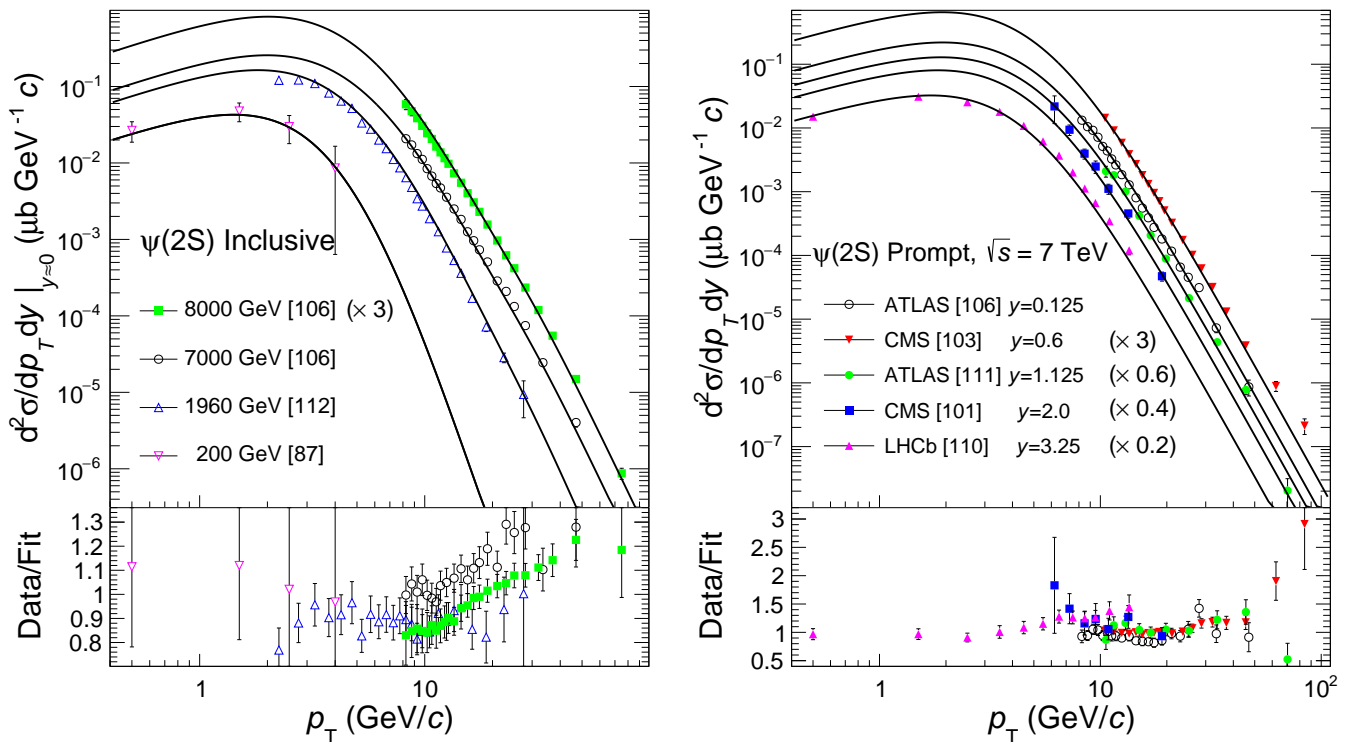


FIG. 14. (color online) Fitting of the $\psi(2S)$ meson cross section vs p_T at mid-rapidity and different \sqrt{s} values (left) and at $\sqrt{s} = 7$ TeV and different rapidity values (right). Data and lines are multiplied by the numbers, indicated in the parentheses, for a better separation.

$0.25 < |y| < 0.5$. As an example of our predictions, Fig. 15 presents the inclusive $\psi(2S)$ meson p_T -integrated (for $p_T > 0$) cross section in pp (also high energy $p\bar{p}$)

collisions versus \sqrt{s} at mid-rapidity and at forward rapidity of $y = 3.25$. Comparison of calculations with the available data shows a reasonable agreement.

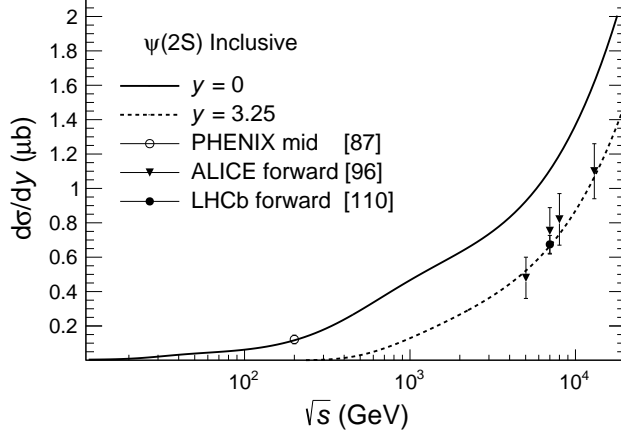


FIG. 15. Inclusive $\psi(2S)$ meson p_T -integrated cross section as a function of \sqrt{s} at mid-rapidity (full line) and forward rapidity of $y = 3.25$ (dashed line) and comparison with the data.

D. $\Upsilon(1S)$, $\Upsilon(2S)$, $\Upsilon(3S)$ mesons

Here, we discuss the fits of Υ -family mesons inclusive production data [93, 102, 104, 105, 113–124] measured at energies \sqrt{s} from 38.8 GeV [113] to 8 TeV [104, 105, 124] in pp collisions and at 1.8 TeV [117] and 1.96 TeV [118] in $p\bar{p}$ collisions. First, a combined fit of more copious $\Upsilon(1S)$ data was done, and the resulting parameter values are given in Table I. Then, separate combined fits were performed for $\Upsilon(2S)$ and $\Upsilon(3S)$ data with free parameters \tilde{V} and p_3 – p_6 , fixing all other parameters to the corresponding values of the $\Upsilon(1S)$ fit. The results for $\Upsilon(2S)$ ($\Upsilon(3S)$) are $\tilde{V} = 0.093 \pm 0.001$ (0.034 ± 0.001) GeV^{-3} , $p_3 = 0.6$ (0.4), $p_4 = 7.5$ (5.8), $p_5 = -8.0$ (–8.0), $p_6 = 0.0548$ (0.0531), $\chi^2/NDF = 3443/491$ (3005/478). Note that such large ratios χ^2/NDF for Υ family are mostly due to the somewhat poor match between results of different LHC experiments. Moreover, two different measurements of the LHCb Collaboration [120, 124] at

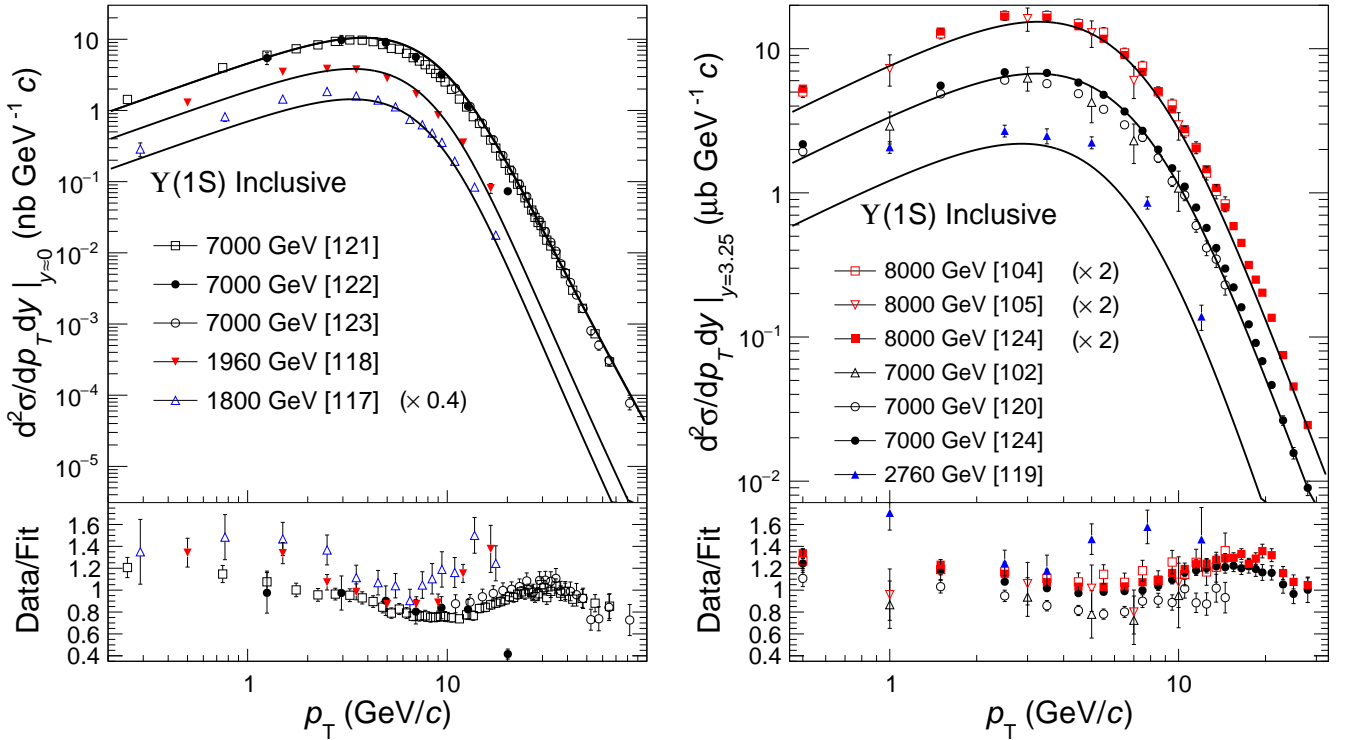


FIG. 16. (color online) Fitting of $\Upsilon(1S)$ meson cross section vs p_T at different \sqrt{s} values for mid-rapidity (left) and forward rapidity of $y = 3.25$ (right). Data and lines at $\sqrt{s} = 1.8, 8$ TeV are multiplied by 0.4, 2, respectively, for a better visibility.

$\sqrt{s} = 7$ TeV do not agree well, and the data at $\sqrt{s} = 2.76$ TeV [119] seem too high with respect to the model predictions (see Figs. 16 and 17).

Examples of inclusive $\Upsilon(1S)$ meson p_T -spectra fits at different \sqrt{s} values are shown in Fig. 16 for mid-rapidity (left) and forward rapidity of $y = 3.25$ (right). Fig. 17

presents the $\Upsilon(1S)$ p_T -integrated cross section (for $p_T > 0$) as a function of y and comparison with the existing measurements at $\sqrt{s} = 2.76$ and 7 TeV. Our prediction for $\sqrt{s} = 13$ TeV is also given. The predictions for this cross section dependence on \sqrt{s} at mid-rapidity and at forward rapidity of $y = 3.25$, together with the available data, are shown in Fig. 18.

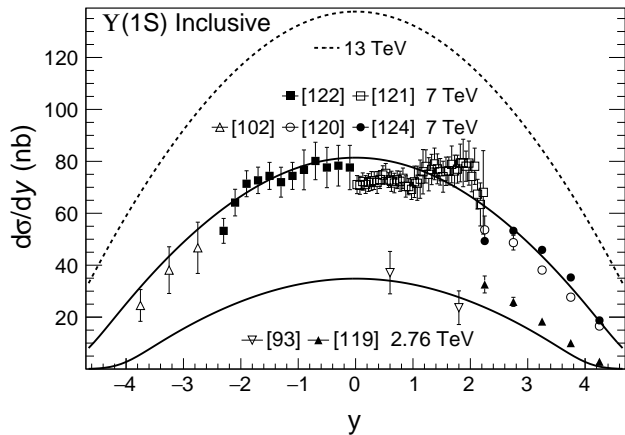


FIG. 17. $\Upsilon(1S)$ meson p_T -integrated cross section as a function of y at different \sqrt{s} values and comparison with the data.

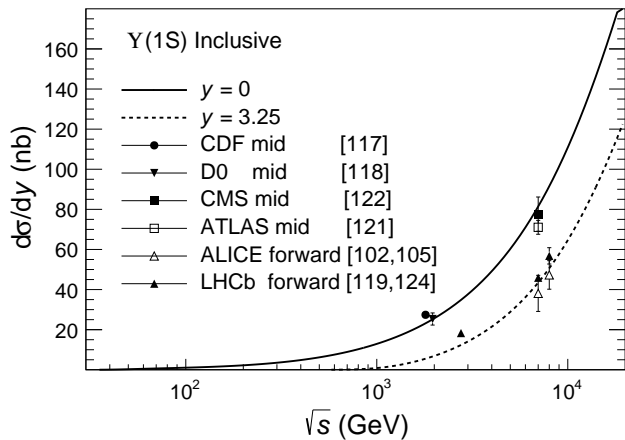


FIG. 18. $\Upsilon(1S)$ meson p_T -integrated cross section as a function of \sqrt{s} at mid-rapidity (full line) and forward rapidity of $y = 3.25$ (dashed line) and comparison with the data.

To illustrate the fits for $\Upsilon(2S)$ and $\Upsilon(3S)$ mesons, we consider the ratios of their inclusive production cross sections times their dimuon branching fractions to the same quantity for $\Upsilon(1S)$, denoted usually as R^{21} and R^{31} , respectively. Figure 19 presents the fit results for the p_T dependence of these ratios at different values of \sqrt{s} and y . Lastly, Fig. 20 demonstrates the model description of the $\Upsilon(1S + 2S + 3S)$ production p_T -integrated cross sec-

tion times the dimuon branching fraction as a function of y , measured in pp collisions at $\sqrt{s} = 200$ GeV [114–116].

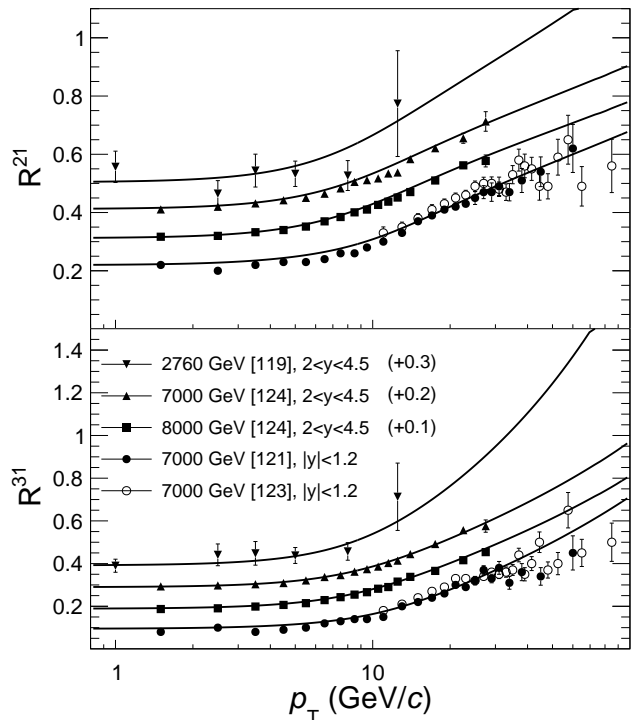


FIG. 19. Fitting of ratios R^{21} and R^{31} vs p_T , described in the text for $\Upsilon(2S)$ and $\Upsilon(3S)$, at different \sqrt{s} and y values. Forward rapidity data and lines at $\sqrt{s} = 8, 7, 2.76$ TeV are shifted up by 0.1, 0.2, 0.3, respectively, for a better separation.

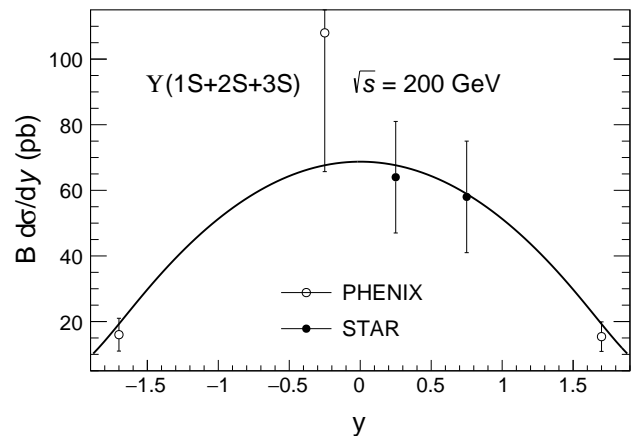


FIG. 20. $\Upsilon(1S + 2S + 3S)$ p_T -integrated cross section times the dimuon branching fraction B versus y for pp collisions at $\sqrt{s} = 200$ GeV and comparison with the data [114–116].

VI. CONCLUSION

Thus, we presented a thermal model of a flowing hadronic fireball, based on the TD and BWM, which describes well almost all available data (except diffractive processes at large y values and some other data sets) on the pion and quarkonia production yields $d^2N/dp_T dy$ in pp collisions at $\sqrt{s} \geq 5$ GeV and in $p\bar{p}$ collisions at $\sqrt{s} > 500$ GeV (where the difference between these two collision types can be neglected). Note that the longitudinal boost invariance is broken in the model due to the used fireball geometry.

One of the distinct features of our model is the assumption that the kinetic freeze-out temperature T is the same for all particle types (while their chemical freeze-out temperatures can differ). T is almost constant at $\sqrt{s} > 500$ GeV, increases with decreasing energy and reaches its maximum at $\sqrt{s} \sim 10$ GeV (see Fig. 2). In this energy region, the parameter n goes to infinity (see Fig. 3) and TD reduces to BGD. Another feature of the model is that the particle chemical potential μ is proportional to its mass and vanishes with increase of \sqrt{s} . The nonzero μ can be interpreted as a measure of the chemical non-equilibrium. Also, we provide parametrizations for the \sqrt{s} dependence of the model parameters allowing predictions for the pion and quarkonia yields in pp or $p\bar{p}$ collisions at new energies of the existing and future accelerators. An example script is given in [125], showing how one can use our model to compute these yields at

any \sqrt{s} , p_T and y in ROOT [57].

In our model, the correlation between the parameters T and q (or n) and radial flow velocity (v_s) has similar behavior as in other models (see, e.g., [5, 23]). Namely, T and q increase with decreasing v_s . A combined fit of the pion data with $v_s = 0$ gives about 10% larger T and from 10% to 70% larger $q - 1$ when moving from the LHC energies down to $\sqrt{s} \sim 20$ GeV. χ^2 of this fit is about 50% larger than the one given in Table I for pions. Quarkonia fits also give similar parameter changes. It can be seen in Eq. (13) that the effect of the radial flow diminishes with increasing rapidity. Owing to this feature, our model describes the experimental fact (see, e.g., [6, 99, 126]) that the p_T spectrum of a given particle becomes softer ($\langle p_T \rangle$ becomes smaller) with the increase of its rapidity.

Finally, since the model includes all the ingredients of the thermal source (fireball), it can be applied for the pion Bose-Einstein correlation studies using, e.g., the methods of [127].

ACKNOWLEDGEMENTS

I thank P. Dupieux, C. Hadjidakis, A. Parvan, O. Teryaev, M. Tokarev and G. Wilk for interest and helpful discussions. I would also like to thank the anonymous referee for important comments and the suggestion to discuss the correlation between the model parameters.

-
- [1] P. Braun-Munzinger, K. Redlich and J. Stachel, *Quark Gluon Plasma 3*, edited by R.C. Hwa and X.-N. Wang (World Scientific, Singapore, 2004), pp. 491-599; A. Andronic, P. Braun-Munzinger and J. Stachel, Nucl. Phys. A **772**, 167 (2006).
 - [2] F. Becattini and G. Passaleva, Eur. Phys. J. C **23**, 551 (2002); F. Becattini, J. Manninen and M. Gazdzicki, Phys. Rev. C **73**, 044905 (2006).
 - [3] J. Cleymans, H. Oeschler, K. Redlich and S. Wheaton, Phys. Rev. C **73**, 034905 (2006); S. Wheaton, J. Cleymans and M. Hauer, Comput. Phys. Commun. **180**, 84 (2009).
 - [4] M. Petran, J. Letessier, J. Rafelski and G. Torrieri, Comput. Phys. Commun. **185**, 2056 (2014); J. Rafelski, Eur. Phys. J. A **51**, 114 (2015).
 - [5] E. Schnedermann, J. Sollfrank and U. Heinz, Phys. Rev. C **48**, 2462 (1993).
 - [6] H. Dobler, J. Sollfrank and U. Heinz, Phys. Lett. B **457**, 353 (1999).
 - [7] M. Chojnacki, A. Kisiel, W. Florkowski and W. Broniowski, Comput. Phys. Commun. **183**, 746 (2012).
 - [8] N.S. Amelin, R. Lednicky, T.A. Pocheptsov, I.P. Lokhtin, L.V. Malinina, A.M. Snigirev *et al.*, Phys. Rev. C **74**, 064901 (2006).
 - [9] S. Tomasik, Comput. Phys. Commun. **180**, 1642 (2009).
 - [10] F. Cooper and G. Frye, Phys. Rev. D **10**, 186 (1974).
 - [11] P. Braun-Munzinger, J. Stachel, J.P. Wessels and N. Xu, Phys. Lett. B **344**, 43 (1995).
 - [12] B.I. Abelev *et al.* (STAR Collaboration), Phys. Rev. C **79**, 034909 (2009).
 - [13] M. Rybczyński, W. Florkowski and W. Broniowski, Phys. Rev. C **85**, 054907 (2012).
 - [14] P. Ghosh, S. Muhuri, J.K. Nayak and R. Varma, J. Phys. G **41**, 035106 (2014).
 - [15] S. Chatterjee, S. Das, L. Kumar, D. Mishra, B. Mohanty *et al.*, Adv. High Energy Phys. **2015**, 349013 (2015).
 - [16] B. Abelev *et al.* (ALICE Collaboration), Phys. Rev. C **88**, 044910 (2013); Phys. Lett. B **728**, 25 (2014).
 - [17] C. Tsallis, J. Stat. Phys. **52**, 479 (1988); C. Tsallis, R.S. Mendes and A.R. Plastino, Physica A **261**, 534 (1998).
 - [18] I. Bediaga, E.M.F. Curado and J.M. de Miranda, Physica A **286**, 156 (2000).
 - [19] C. Beck, Physica A **286**, 164 (2000); **305**, 209 (2002); Eur. Phys. J. A **40**, 267 (2009).
 - [20] G. Wilk and Z. Włodarczyk, Phys. Rev. Lett. **84**, 2770 (2000).
 - [21] G. Wilk and Z. Włodarczyk, Eur. Phys. J. A **40**, 299 (2009); Phys. Rev. C **79**, 054903 (2009).
 - [22] T.S. Biró, G. Purcsel and K. Ürmösy, Eur. Phys. J. A **40**, 325 (2009).
 - [23] Z. Tang, Y. Xu, L. Ruan, G. van Buren, F. Wang and Z. Xu, Phys. Rev. C **79**, 051901 (2009); K. Jiang, Y. Zhu, W. Liu, H. Chen, C. Li, L. Ruan *et al.*, Phys. Rev. C **91**, 024910 (2015).

- [24] J.M. Conroy, H.G. Miller and A.R. Plastino, Phys. Lett. A **374**, 4581 (2010).
- [25] J. Cleymans and D. Worku, J. Phys. G **39**, 025006 (2012); Eur. Phys. J. A **48**, 160 (2012).
- [26] J. Cleymans, G.I. Lykasov, A.S. Parvan, A.S. Sorin, O.V. Teryaev and D. Worku, Phys. Lett. B **723**, 351, 2013; A.S. Parvan, O.V. Teryaev and J. Cleymans, arXiv:1607.01956 [hep-ph] (2016).
- [27] M.D. Azmi and J. Cleymans, J. Phys. G **41**, 065001 (2014); Eur. Phys. J. C **75**, 430 (2015).
- [28] M. Rybczyński and Z. Włodarczyk, Eur. Phys. J. C **74**, 2785 (2014).
- [29] C.-Y. Wong and G. Wilk, Acta Phys. Polon. B **43**, 2047 (2012).
- [30] C.-Y. Wong and G. Wilk, Phys. Rev. D **87**, 114007 (2013).
- [31] C.-Y. Wong, G. Wilk, L.J.L. Cirto and C. Tsallis, Phys. Rev. D **91**, 114027, (2015).
- [32] G. Wilk and Z. Włodarczyk, Physica A **413**, 53 (2014); Acta Phys. Polon. B **46**, 1103 (2015).
- [33] M. Rybczyński, G. Wilk and Z. Włodarczyk, Eur. Phys. J. Web Conf. **90**, 01002 (2015).
- [34] K. Ürmösy, arXiv:1212.0260 [hep-ph] (2012).
- [35] G. Wilk and Z. Włodarczyk, Phys. Lett. A **379**, 2941 (2015).
- [36] B.-C. Li, Y.-Z. Wang, F.-H. Liu, X.-J. Wen and Y.-E. Dong, Phys. Rev. D **89**, 054014 (2014).
- [37] I. Sena and A. Deppman, Eur. Phys. J. A **49**, 17 (2013); AIP Conf. Proc. **1520**, 172 (2013).
- [38] E. Megías, D.P. Menezes and A. Deppman, Physica A **421**, 15 (2015).
- [39] L. Marques, J. Cleymans and A. Deppman, Phys. Rev. D **91**, 054025 (2015).
- [40] H. Zheng, L. Zhu and A. Bonasera, Phys. Rev. D **92**, 074009 (2015).
- [41] D. Thakur, S. Tripathy, P. Garg, R. Sahoo and J. Cleymans, Adv. High Energy Phys. **2016**, 4149352 (2016).
- [42] K. Ürmösy *et al.*, arXiv:1501.02352 [hep-ph] (2015); G. Biró *et al.*, Entropy **19**, 88 (2017).
- [43] B.I. Abelev *et al.* (STAR Collaboration), Phys. Rev. C **75**, 064901 (2007).
- [44] A. Adare *et al.* (PHENIX Collaboration), Phys. Rev. D **83**, 052004 (2011).
- [45] A. Adare *et al.* (PHENIX Collaboration), Phys. Rev. C **83**, 064903 (2011).
- [46] V. Khachatryan *et al.* (CMS Collaboration), Phys. Rev. Lett. **105**, 022002 (2010).
- [47] G. Aad *et al.* (ATLAS Collaboration), New J. Phys. **13**, 053033 (2011).
- [48] J. Adam *et al.* (ALICE Collaboration), Eur. Phys. J. C **75**, 226 (2015).
- [49] Yu.M. Sinyukov, S.V. Akkelin and A.Yu. Tolstykh, Nukleonika **43**, 369 (1998).
- [50] J. Sollfrank, Eur. Phys. J. C **9**, 159 (1999).
- [51] U. Heinz, J. Phys. G **25**, 263 (1999).
- [52] J. Cleymans and K. Redlich, Phys. Rev. C **60**, 054908 (1999).
- [53] W. Broniowski and W. Florkowski, Phys. Rev. Lett. **87**, 272302 (2001).
- [54] S.V. Akkelin, P. Braun-Munzinger and Yu.M. Sinyukov, Nucl. Phys. A **710**, 439 (2002).
- [55] A. Erdélyi *et al.*, *Higher Transcendental Functions* (McGraw-Hill, New York, 1953), Vol. 1, Chap. 3.
- [56] M.J. Menon and P.V.R.G. Silva, J. Phys. G **40**, 125001 (2013); **41**, 019501 (2014) [Erratum].
- [57] R. Brun and F. Rademakers, Nucl. Instrum. Methods Phys. Res. Sect. A **389**, 81 (1997); <http://root.cern.ch>.
- [58] C. Kourkouvelis *et al.*, Z. Phys. C **5**, 95 (1980).
- [59] A. Adare *et al.* (PHENIX Collaboration), Phys. Rev. D **79**, 012003 (2009).
- [60] A. Adare *et al.* (PHENIX Collaboration), Phys. Rev. D **76**, 051106 (2007).
- [61] B.I. Abelev *et al.* (STAR Collaboration), Phys. Rev. D **80**, 111108 (2009).
- [62] L. Adamczyk *et al.* (STAR Collaboration), Phys. Rev. D **89**, 012001 (2014).
- [63] A. Adare *et al.* (PHENIX Collaboration), Phys. Rev. D **93**, 011501(R) (2016).
- [64] M. Banner *et al.* (UA2 Collaboration), Phys. Lett. B **115**, 59 (1982); Z. Phys. C **27**, 329 (1985).
- [65] B. Abelev *et al.* (ALICE Collaboration), Phys. Lett. B **717**, 162 (2012).
- [66] S. Acharya *et al.* (ALICE Collaboration), arXiv:1702.00917 [hep-ex] (2017).
- [67] V. Blobel *et al.* (Bonn-Hamburg-München Collaboration), Nucl. Phys. B **69**, 454 (1974).
- [68] E.W. Beier *et al.*, Phys. Rev. Lett. **37**, 1114 (1976).
- [69] N. Abgrall *et al.* (NA61/SHINE Collaboration), Eur. Phys. J. C **74**, 2794 (2014).
- [70] B. Alper *et al.*, Nucl. Phys. B **100**, 237 (1975).
- [71] J. Adams *et al.* (STAR Collaboration), Phys. Lett. B **637**, 161 (2006).
- [72] M. Banner *et al.* (UA2 Collaboration), Phys. Lett. B **122**, 322 (1983).
- [73] K. Aamodt *et al.* (ALICE Collaboration), Eur. Phys. J. C **71**, 1655 (2011).
- [74] B. Abelev *et al.* (ALICE Collaboration), Phys. Lett. B **736**, 196 (2014).
- [75] C. Alt *et al.* (NA49 Collaboration), Eur. Phys. J. C **45**, 343 (2006).
- [76] I. Arsene *et al.* (BRAHMS Collaboration), Phys. Rev. Lett. **98**, 252001 (2007).
- [77] S.V. Afanasiev *et al.* (NA49 Collaboration), Phys. Lett. B **491**, 59 (2000); T. Anticic *et al.* (NA49 Collaboration), Eur. Phys. J. C **68**, 1 (2010).
- [78] A. Adare *et al.* (PHENIX Collaboration), Phys. Rev. D **90**, 052002 (2014).
- [79] K. Aamodt *et al.* (ALICE Collaboration), Eur. Phys. J. C **71**, 1594 (2011).
- [80] J. Adam *et al.* (ALICE Collaboration), Phys. Lett. B **768**, 203 (2017); arXiv:1702.00555 [nucl-ex] (2017).
- [81] R. Aaij *et al.* (LHCb Collaboration), Phys. Lett. B **703**, 267 (2011).
- [82] B. Abelev *et al.* (ALICE Collaboration), Eur. Phys. J. C **72**, 2183 (2012).
- [83] B. Abelev *et al.* (ALICE Collaboration), Phys. Lett. B **710**, 557 (2012).
- [84] T. Aaltonen *et al.* (CDF Collaboration), Phys. Rev. D **88**, 092005 (2013).
- [85] T. Alexopoulos *et al.* (E735 Collaboration), Z. Phys. C **67**, 411 (1995).
- [86] J. Badier *et al.* (NA3 Collaboration), Z. Phys. C **20**, 101 (1983).
- [87] A. Adare *et al.* (PHENIX Collaboration), Phys. Rev. D **85**, 092004 (2012).
- [88] L. Adamczyk *et al.* (STAR Collaboration), Phys. Lett. B **722**, 55 (2013).

- [89] F. Abe *et al.* (CDF Collaboration), Phys. Rev. Lett. **79**, 572 (1997).
- [90] B. Abbott *et al.* (D0 Collaboration), Phys. Rev. Lett. **82**, 35 (1999).
- [91] D. Acosta *et al.* (CDF Collaboration), Phys. Rev. D **66**, 092001 (2002).
- [92] D. Acosta *et al.* (CDF Collaboration), Phys. Rev. D **71**, 032001 (2005).
- [93] S. Chatrchyan *et al.* (CMS Collaboration), JHEP **05**, 063 (2012).
- [94] B. Abelev *et al.* (ALICE Collaboration), Phys. Lett. B **718**, 295 (2012); **748**, 472 (2015) [Erratum].
- [95] R. Aaij *et al.* (LHCb Collaboration), JHEP **02**, 041 (2013).
- [96] J. Adam *et al.* (ALICE Collaboration), arXiv:1702.00557 [hep-ex] (2017).
- [97] V. Khachatryan *et al.* (CMS Collaboration), Eur. Phys. J. C **71**, 1575 (2011).
- [98] G. Aad *et al.* (ATLAS Collaboration), Nucl. Phys. B **850**, 387 (2011).
- [99] R. Aaij *et al.* (LHCb Collaboration), Eur. Phys. J. C **71**, 1645 (2011); **73**, 2631 (2013).
- [100] K. Aamodt *et al.* (ALICE Collaboration), Phys. Lett. B **704**, 442 (2011); **718**, 692 (2012) [Erratum]; B. Abelev *et al.* (ALICE Collaboration), JHEP **11**, 065 (2012).
- [101] S. Chatrchyan *et al.* (CMS Collaboration), JHEP **02**, 011 (2012).
- [102] B. Abelev *et al.* (ALICE Collaboration), Eur. Phys. J. C **74**, 2974 (2014).
- [103] V. Khachatryan *et al.* (CMS Collaboration), Phys. Rev. Lett. **114**, 191802 (2015).
- [104] R. Aaij *et al.* (LHCb Collaboration), JHEP **06**, 064 (2013);
- [105] J. Adam *et al.* (ALICE Collaboration), Eur. Phys. J. C **76**, 184 (2016).
- [106] G. Aad *et al.* (ATLAS Collaboration), Eur. Phys. J. C **76**, 283 (2016).
- [107] R. Aaij *et al.* (LHCb Collaboration), JHEP **10**, 172 (2015).
- [108] C. Albajar *et al.* (UA1 Collaboration), Phys. Lett. B **256**, 112 (1991).
- [109] C. Kourkoumelis *et al.*, Phys. Lett. **91B**, 481 (1980).
- [110] R. Aaij *et al.* (LHCb Collaboration), Eur. Phys. J. C **72**, 2100 (2012).
- [111] G. Aad *et al.* (ATLAS Collaboration), JHEP **09**, 079 (2014).
- [112] T. Aaltonen *et al.* (CDF Collaboration), Phys. Rev. D **80**, 031103(R) (2009).
- [113] L.Y. Zhu *et al.* (E866/NuSea Collaboration), Phys. Rev. Lett. **100**, 062301 (2008).
- [114] A. Adare *et al.* (PHENIX Collaboration), Phys. Rev. C **87**, 044909 (2013).
- [115] L. Adamczyk *et al.* (STAR Collaboration), Phys. Lett. B **735**, 127 (2014).
- [116] A. Adare *et al.* (PHENIX Collaboration), Phys. Rev. C **91**, 024913 (2015).
- [117] D. Acosta *et al.* (CDF Collaboration), Phys. Rev. Lett. **88**, 161802 (2002).
- [118] V.M. Abazov *et al.* (D0 Collaboration), Phys. Rev. Lett. **94**, 232001 (2005); **100**, 049902 (2008) [Erratum].
- [119] R. Aaij *et al.* (LHCb Collaboration), Eur. Phys. J. C **74**, 2835 (2014).
- [120] R. Aaij *et al.* (LHCb Collaboration), Eur. Phys. J. C **72**, 2025 (2012).
- [121] G. Aad *et al.* (ATLAS Collaboration), Phys. Rev. D **87**, 052004 (2013).
- [122] S. Chatrchyan *et al.* (CMS Collaboration), Phys. Lett. B **727**, 101 (2013).
- [123] V. Khachatryan *et al.* (CMS Collaboration), Phys. Lett. B **749**, 14 (2015).
- [124] R. Aaij *et al.* (LHCb Collaboration), JHEP **11**, 103 (2015).
- [125] <https://www.dropbox.com/s/5zocgyqafh7avpe/yields.C>.
- [126] I.G. Bearden *et al.* (BRAHMS Collaboration), Phys. Rev. Lett. **94**, 162301 (2005).
- [127] A. Bialas, W. Florkowski and K. Zalewski, Acta Phys. Pol. B **45**, 1883 (2014); J. Phys. G **42**, 045001 (2015).